Biosensors and Bioelectronics 263 (2024) 116620

Contents lists available at ScienceDirect

Biosensors and Bioelectronics

journal homepage: www.elsevier.com/locate/bios

Exploiting CO_2 laser to boost graphite inks electron transfer for fructose biosensing in biological fluids

Filippo Silveri [a], Flavio Della Pelle [a,*], Annalisa Scroccarello [a], Paolo Bollella [b], Giovanni Ferraro [c], Eole Fukawa [d], Yohei Suzuki [d], Keisei Sowa [d], Luisa Torsi [b], Dario Compagnone [a,**]

[a] Department of Bioscience and Technology for Food, Agriculture and Environment, University of Teramo, Campus "Aurelio Saliceti" Via R. Balzarini 1, 64100, Teramo, Italy
[b] Department of Chemistry, University of Bari Aldo Moro, Via E. Orabona 4, 70125, Bari, Italy
[c] Department of Chemistry "Ugo Schiff" and CSGI, University of Florence, Via Della Lastruccia 3, Sesto Fiorentino, 50019, Florence, Italy
[d] Division of Applied Life Sciences, Graduate School of Agriculture, Kyoto University, Kitashirakawa Oiwake-cho, Sakyo-ku, Kyoto, 606-8502, Japan

ARTICLE INFO

Keywords:
Electrochemical sensors
Biosensors
Biological fluids analysis
CO_2-Laser
Carbon-based inks

ABSTRACT

The possibility to print electronics by means of office tools has remarkedly increased the possibility to design affordable and robust point-of-care/need devices. However, conductive inks suffer from low electrochemical and rheological performances limiting their applicability in biosensors. Herein, a fast CO_2 laser approach to activate printed carbon inks towards direct enzymatic bioelectrocatalysis (3rd generation) is proposed and exploited to build biosensors for D-fructose analysis in biological fluids.

The CO_2 laser treatment was compared with two lab-grade printed transducers fabricated with solvent (SB) and water (WB) based carbon inks. The use of the laser revealed significant morpho-chemical variations on the printed inks and was investigated towards enzymatic direct catalysis, using Fructose dehydrogenase (FDH) integrated into entirely lab-produced biosensors. The laser-driven activation of the inks unveils the inks' direct electron transfer (DET) ability between FDH and the electrode surface. Sub-micromolar limits of detection (SB-ink LOD = 0.47 μM; WB-ink LOD = 0.24 μM) and good linear ranges (SB-ink: 5–100 μM; WB-ink: 1–50 μM) were obtained, together with high selectivity due to use of the enzyme and the low applied overpotential (0.15 V vs. pseudo-Ag/AgCl). The laser-activated biosensors were successfully used for D-fructose determination in complex synthetic and real biological fluids (recoveries: 93–112%; RSD ≤8.0%, n = 3); in addition, the biosensor ability for continuous measurement (1.5h) was also demonstrated simulating physiological D-fructose fluctuations in cerebrospinal fluid.

1. Introduction

Nowadays, printed electronics is worldwide recognized as a smart approach for the production of flexible and wearable electronics. Different printing technologies have been proposed including flexographic, offset, gravure, inkjet, and screen-printing (Dimitriou and Michailidis, 2021; Martins et al., 2023; Suresh et al., 2021). Among others, stencil printing has attracted increasing attention, offering the possibility to produce on-demand designs just using a cutting-plotter, allowing every lab to produce in-series sensors and electronic devices (Kay and Desmulliez, 2012; Kongkaew et al., 2022; Silveri et al., 2023a, 2023b). Regardless of the technique employed, the electronics' features are strongly affected by the used ink. Graphite-based inks are commonly used for the development of electrochemical sensors due to their low cost and for mechanical, thermal, and chemical features, that allow different printing approaches on different substrates (Camargo et al., 2021). However, despite their widespread use, the presence of binders and/or stabilizers in the formulation often results in poor electron-transfer ability and reduced-exposed active surface, making 'pristine' graphitic inks not always suitable for electro-analytical purposes (Rocha et al., 2021; Yuan et al., 2021).

Beyond the widely used post-printing modifications using

* Corresponding author.
** Corresponding author.
E-mail addresses: fdellapelle@unite.it (F. Della Pelle), dcompagnone@unite.it (D. Compagnone).

https://doi.org/10.1016/j.bios.2024.116620
Received 30 May 2024; Received in revised form 8 July 2024; Accepted 30 July 2024
Available online 31 July 2024

nanomaterials, several efforts have been devoted to find fast and effective strategies to directly boost printed-inks performance. Chemical, electrochemical, and plasma-based treatments have been proposed (Cheunkar et al., 2022; Silva et al., 2019; Yuan et al., 2021; Zappi et al., 2021). These approaches require time-consuming post-printing steps and often need the use of toxic/hazardous chemicals and dedicated instrumentation. These methods generally change only the ink's surface chemistry, not driving useful morphological changes such as nanostructuration and/or removal of printing additives. Therefore, the search for effective strategies to enhance electroanalytical features is still on course, while methods to induce/activate interactions between printed inks and biological elements deserve to be further studied.

Recently, CO_2 laser-based strategies to induce carbon-based materials nano/micro-structuration and 'tuning' have grown exponentially in the electroanalytical field. Laser technologies take advantage of the photothermal energy released by the laser beam (IR emission) which, in case of photosensitive substrates, leads to instantaneous morpho-chemical changes (Griffiths et al., 2014; You et al., 2020). These changes can lead to conductive circuits and nanostructure formations and heterostructures/hybrid-nanomaterials assembling (Della Pelle et al., 2023; Scroccarello et al., 2023; Silveri et al., 2023b); moreover, the laser can be also used for 3D-printed electrodes 'sintering' (Rocha et al., 2021; Veloso et al., 2023). Overall, properly conducted CO_2 laser treatments can generate and/or improve electrochemical features of different kinds of carbonaceous substrates, thus representing an appealing opportunity for (bio)analytical device development.

In the printed electronics field, pioneering works have explored the CO_2 laser effect on screen-printed electrodes, demonstrating the ability to induce favorable morpho-chemical changes (Alba et al., 2021a, 2021b). Further studies have employed laser-treated printed electrodes to build up electrochemiluminescence-based devices (Alba et al., 2022) and supercapacitors (Baptista et al., 2022). In this framework, our group employed laser treatments to induce gold nanoparticles formation in carbon ink (Silveri et al., 2023b). Despite the intriguing preliminary outcomes, additional efforts should be devoted to understand the mechanism and potentiality of these laser treatments. For instance, laser technology on water-based inks has not been explored yet, even though water-based formulations represent a turning point for developing more sustainable printed devices (Camargo et al., 2021; Marchianò et al., 2024; Sanchez-Duenas et al., 2023; Tricase et al., 2023). Furthermore, the potential of laser-treated printed circuits in the bioelectronics field has not been explored, especially regarding the interaction with biological elements as redox enzymes, despite the laser approach being fast and scalable at an industrial level.

Bioelectronics deal with the integration of bioelements as active components of electronic devices; among biomolecules, redox enzymes have gained significant attention for their catalytic functions (Camargo et al., 2021; Marchianò et al., 2024; Sanchez-Duenas et al., 2023; Tricase et al., 2023). Among them, some are able to directly communicate with electrodes, resulting in direct electron transfer (DET) phenomena (Bollella, 2022; Schachinger et al., 2021). DET is at the basis of biofuel cells and 3rd generation enzymatic biosensors, which exploit the direct electrons shuttling between the redox site of the protein and the transducer surface (Adachi et al., 2020). Fructose dehydrogenase (FDH), a membrane-bound flavohemo-protein responsible for the conversion of D-fructose in 5-keto-D-fructose throughout a $2H^+/2e^-$ oxidation, is capable to give DET if faced with properly engineered electrodic surfaces (Fukawa et al., 2024; Suzuki et al., 2023). Indeed, FDH has been employed to build up electrochemical biosensors (Bollella, 2022), where DET is generally favored by the enzyme orientation and employing additional nanomaterials or dedicated nanostructured surfaces (Bollella, 2022; Bollella and Katz, 2020); however, the latter approaches often make the biosensor realization time-consuming, cumbersome and hardly automatable. FDH-biosensors have been mainly employed for D-fructose determination in food samples, whereas the applicability in the biomedical field is still not widely explored, although the evidence of D-fructose impact on human health, in particularly for vulnerable subjects such as infants or diabetic patients (Andres-Hernando et al., 2019; Hwang et al., 2017; Li et al., 2018; Singh and Sarma, 2022; Tigchelaar et al., 2022).

In this work, a CO_2 laser strategy to activate printed carbon-ink transducers towards DET-based bioelectrocatalysis is proposed. Two inks with different formulations have been considered, one solvent-based (SB) and the other water-based (WB), building up fully integrated lab-manufactured fructose dehydrogenase-based DET-type biosensors; these were used for D-fructose analysis in synthetic and real biological fluids. The laser-induced changes were morpho-chemically evaluated, and correlated with the electrochemical features, with particular regard to the FDH-catalytic event. Raman and FTIR spectroscopy together with scanning electron microscopy were employed, parametrizing the corresponding electron-transfer and biocatalytic implications. The laser effect was also evaluated towards the lab-made ink-activated FDH 3rd generation biosensors analytical features. Biosensors were employed for the determination of D-fructose in formulated and donkey milk, and in artificial seminal and cerebrospinal fluid, proving accuracy and selectivity; eventually, the biosensors' ability to measure in continuous in complex media was proved to simulate D-fructose fluctuations in cerebrospinal fluid.

2. Experimental section

2.1. Materials, chemicals and samples

Solvent-based carbon graphite ink (SB-ink), water-based conductive graphite ink for flexographic printing (WB-ink), Ag/AgCl ink were purchased from Sigma Aldrich (St Louis MO, USA). Recombinant D-fructose dehydrogenase (FDH; native EC 1.1.99.11 from *Gluconobacter japonicus* NBRC 3260, 40 U mg^{-1}) was expressed and purified according to Kawai et al. (2013) and stored in sodium phosphate buffer (pH 6.0, 0.1% Triton® X-100, and 1 mM 2-mercaptoethanol).

The complete list of chemicals, materials, and samples is reported in *section SM.2.1*.

2.2. Apparatus

A detailed description is reported in *section SM.2.2*.

2.3. Biosensors manufacturing and CO_2 laser-activation

The biosensor manufacturing is summarized in Scheme 1. Firstly, the patterned stencil mask was stuck onto the PET sheet and then the ink was spread with a squeegee, ensuring the formation of working, counter and reference electrodes. The curing of the inks was performed following the manufacturer's recommendations at 60 °C for 30 min and 10 min for SB-ink and WB-ink, respectively. To obtain a complete electrochemical cell, Ag/AgCl ink was smoothly brushed onto the reference electrode, followed by curing at 60 °C for 10 min. The transducers' working area was insulated from the contacts laminating a complementary PET-EVA sheet using a thermal roll laminator. The laser activation of the printed ink-based working electrodes was performed using the CO_2 laser plotter in engraving mode (7.4 cm focusing lens); laser details are reported in *section SM.2.2.* The treatment was performed at a laser source power of 4.8 W and 3.6 W for SB-ink and WB-ink respectively, using a laser speed of 1.50 m s^{-1}. Eventually, the biosensors were completed depositing 15 mU of FDH onto the working electrode surface and left to interact for 45 min in the dark.

2.4. Morpho-chemical characterization

A detailed description of SEM, Raman and FT-IR analysis is reported in *section SM.2.4*.

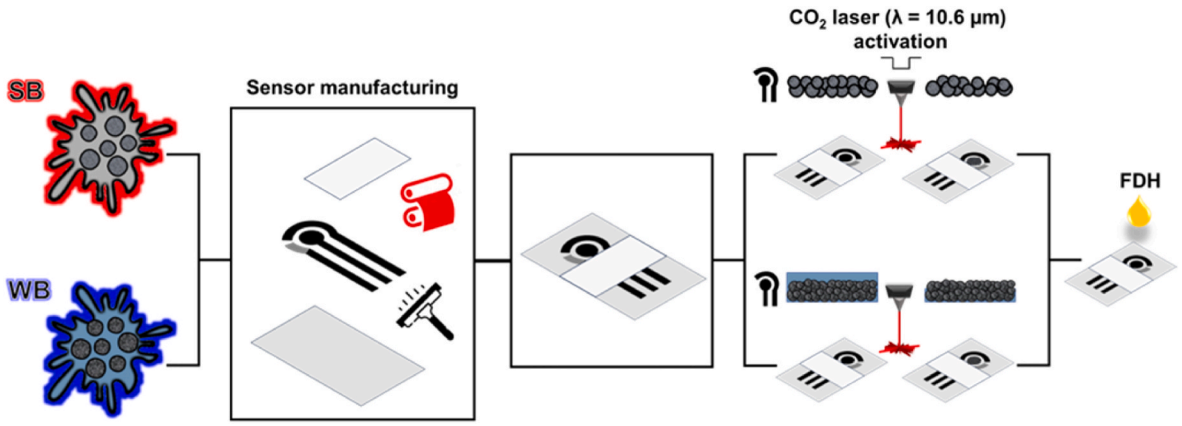

Scheme 1. Sketch of biosensors manufacturing procedure. Printing of the ink-based transducers, CO_2-laser activation of the SB and WB printed inks, and FDH-functionalization of the laser-activated working electrode.

2.5. Electrochemical and electrocatalytic measurements

Electrochemical features of the ink-based transducers were investigated via cyclic voltammetry (CV) at 25 mV s^{-1} using 5 mM $[Fe(CN)_6]^{3-/4-}$ in 0.1 M KCl. CV at 25 mV s^{-1} was further employed to explore the response of 1 mM ascorbic acid, 1 mM caffeic acid, and 1 mM dopamine in 0.1 M phosphate buffer pH = 7. Double layer capacitance (C_s) investigation was performed via CV at increasing scan rates in 0.1 M KOH, working in the non-faradic potential window. DET reaction with FDH was investigated performing CVs at 5 mV s^{-1} in 50 mM acetate buffer pH = 4.5 containing 0.1 M KCl, in absence and presence of 10 mM D-fructose. CV experiments were conducted employing external counter (CE) and reference (RE) electrodes, using a Pt-wire and Ag/AgCl (3 M KCl), respectively. Amperometry was employed for D-fructose biosensing, using +0.15 V as overpotential (vs. pseudo-Ag/AgCl); for these experiments, the integrated biosensors were employed (*section 2.3*).

2.6. D-fructose determination in biological fluids

D-fructose determination in powder formula milk, donkey milk, artificial seminal fluid (aSF), and synthetic cerebrospinal fluid (CSF) was performed via amperometry (+0.15 V vs. pseudo-Ag/AgCl); the samples were diluted in acetate buffer to fit the linear range, and D-fructose was quantified using standard additions method.

Continuous measurement to simulate the D-fructose fluctuations in cerebrospinal fluid was carried out by placing the biosensor in a 10 mL vessel, connected with two inlet tubes and one outlet tube whose flows were controlled by a peristaltic pump. The inlets were connected to 'mobile phases' containing D-fructose in CSF (phase A) and acetate buffer (phase B), respectively. Two different types of D-fructose fluctuation were simulated for the biosensors based on SB-ink and WB-ink, in both cases, amperometry was employed (+0.15 V vs. pseudo-Ag/AgCl); the detailed phases gradients applied along the 1.5 h of measure are reported in *section SM.2.6*.

3. Results and discussion

The idea behind this work was to explore the potentiality of CO_2 laser to activate printed graphitic inks' direct electron transfer (DET) ability toward the redox enzyme fructose dehydrogenase (FDH), to obtain performing 3rd generation fructose biosensors. The full list of the experiments carried out is resumed in Scheme S1. The effect of the laser treatment on water-based and solvent-based inks was carefully investigated. The influence of the laser power on the inks was investigated via the redox probe $[Fe(CN)_6]^{3-/4-}$ and Raman spectroscopy, to understand the electron-transfer abilities and morpho-chemical changes induced by the treatment (*section 3.1*). The bio-catalytic event vs. laser power as a function of the DET reaction kinetics and D-fructose biosensing was studied (*section 3.2*). A complete electrochemical characterization, including the study of additional redox-active compounds, has been also performed to have an overview of the laser treatment effect (*section S3.1*). Eventually, the laser-activated biosensors were applied for the D-fructose determination/monitoring in surrogate breastfeeding milk and synthetic biological fluids.

3.1. CO_2 laser-activation of printed inks. Physico-chemical and electrochemical characterization

Solvent (SB) and water-based (WB) ink printing and sensor manufacturing are resumed in Scheme 1 and explained in detail in *section 2.3*.

The influence of the laser treatment on physical, chemical, and electrochemical features of the two printed inks was explored. To this aim, SB and WB transducers were treated applying laser power between 1.2 and 6.0 W. For each treatment cyclic voltammetry (CV) with the inner-sphere redox probe $[Fe(CN)_6]^{3-/4-}$ was recorded. Fig. 1A and 1B displays the intensity of the faradaic density current obtained treating the SB and WB transducers, respectively; the voltammograms are reported in Fig. S1.

The treatment revealed a current density increase with respect to the applied power. Two different trends were observed: SB-ink is characterized by a 'two-steps' current increasing process, reaching a plateau between 2.4 and 4.8 W, then decrease at 6 W. The treatment at 4.8 W returned a more reproducible response (RSD = 2.2%, n = 3). On the other hand, WB-ink shows an exponential-like behavior, reaching the maximum faradaic current density at 3.6 W (RSD = 0.2%, n = 3). Applying higher power, a significant decrease of performance is observed, up to 6 W where the printed ink stops working. This phenomenon is caused by the excessive energy of the treatment that leads to the local burning and displacement of the films.

Fig. 1C and 1D report Raman spectra obtained treating the SB and WB inks with different laser power (0, 1.2, 1.8, 2.4, 3.6, 4.8, 6.0 W). All spectra have two sharp and clearly separated peaks, corresponding to the typical graphitic carbon D-band (~1350 cm^{-1}) and G-band (~1600 cm^{-1}). The D-band gives information on primary in-plane vibrations of sp^3 carbon and its relative intensity is used to estimate the degree of defects, while the G-band arises from the stretching of the C=C sp^2 bonds (Alba et al., 2021a; Ferrari, 2007; Ma et al., 2019).

From the spectra, it is evident how the laser affects the morpho-chemical features of the materials, and this effect is dependent of the ink type and applied laser power. In particular, SB-ink shows a linear decrease of the I_D/I_G ratio according to the increase of the laser power (Fig. 1C inset). This result indicates that the reduction of the structural disorder is proportional to the laser power (Alba et al., 2021a, 2021b).

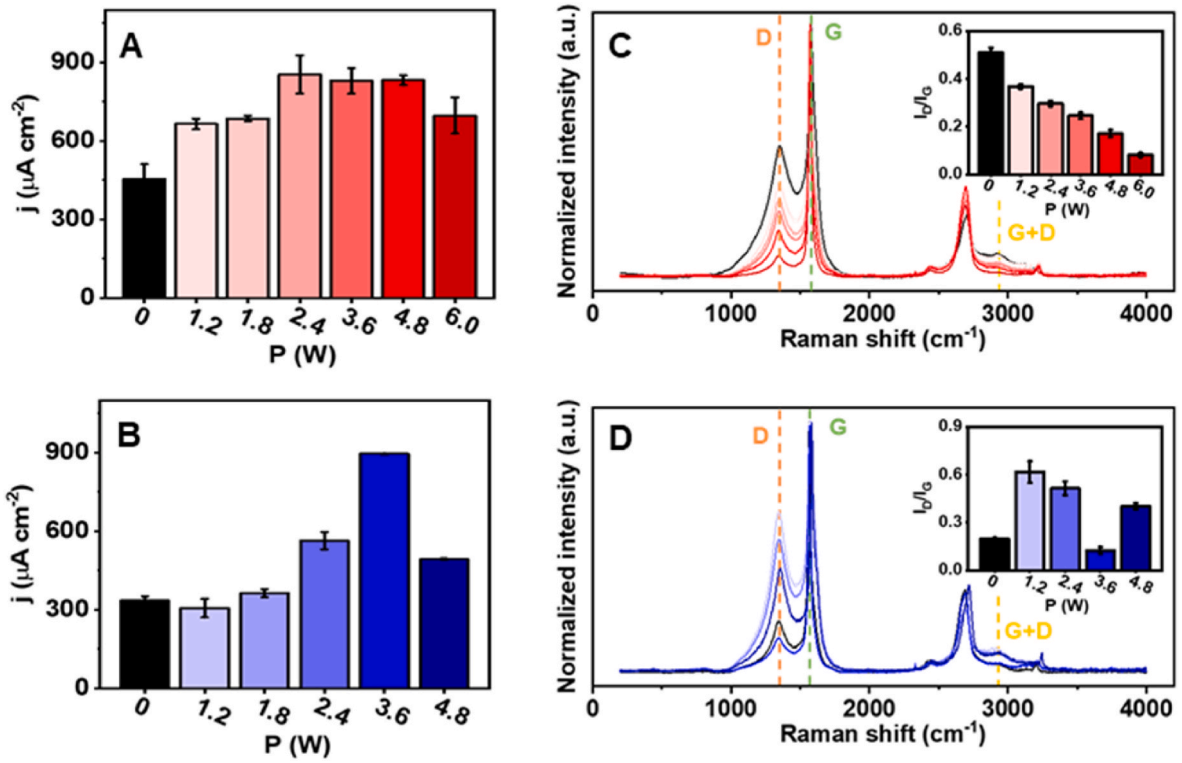

Fig. 1. Faradaic current densities extrapolated from ferro/ferricyanide cyclic voltammograms obtained for SB (**A**) and WB (**B**) ink transducers treated with different laser beam powers. Raman spectra for SB (**C**) and WB (**D**) inks treated with increasing laser power; the insets report the relative values of the extrapolated I_D/I_G ratio. Red and blue shades stand for SB-ink and WB-ink, respectively; the laser power increase is indicated by the relative color darkening. Black bars (A–B) and curves (C–D) indicate the pristine ink-printed transducers (not subjected to laser treatment).

On the other hand, WB-ink shows a slightly different trend, since the untreated ink displays a significantly lower I_D/I_G ratio (Fig. 1D inset) compared to the first laser power applied (1.2 W) and the I_D/I_G ratio decreases up to 3.6 W. This trend is in agreement with the current density trend discussed before. The native WB-ink I_D/I_G low value may be attributed to the production of a more ordered external layer after the printing, which is subsequently removed by the laser treatment exposing the carbon graphitic matrix (this peculiar behavior will be further discussed in this section). Interestingly, Raman spectra for both inks exhibit two additional peaks at higher wavelengths, i.e., the 2D band (~2700 cm^{-1}) related to the presence of a multilayered graphitic structure, and the G + D band (~2950 cm^{-1}) related to structural defects (Ma et al., 2019). The latter band decreases with the applied laser power further confirming that the treatment drives defects removal; regardless of the expected printed material differences, the two inks showed similar behavior toward laser power.

To shed light on the morphological effect of the laser treatment, pristine printed inks have been compared with the laser-treated ones via scanning electron microscopy; in this case, the more promising laser power was investigated, i.e., 4.8 W and 3.6 W for SB and WB ink, respectively. Fig. 2 reports the pictures of treated and untreated inks together with SEM micrographs at different magnifications.

SEM micrographs demonstrate the laser-driven morphological changes of the inks: Fig. 2A of SB-ink reveals the presence of wide graphite flakes interspersed among carbon nanoparticles (ii); the flakes undergo fragmentation phenomena after the laser treatment, inducing the formation of wrinkled flakes with more jagged edges completely covered with carbon nanoparticles, resulting in a flower-like morphology (iii) suggesting a larger exposed area. Fig. 2B of WB-ink shows unresolved carbon nanoparticles immersed in a continuous 'patina' (ii), attributable to the polymer resins commonly used for flexographic printing (Pranav Y. Dave, 2020). The laser treatment induces the

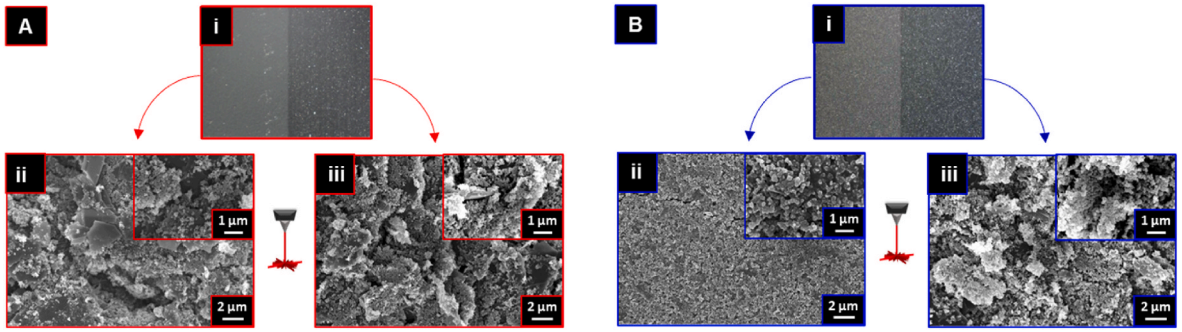

Fig. 2. Morphological characterization of pristine and laser-activated SB (**A**) and WB (**B**) ink-based transducer surfaces. (**i**) Optical pictures of the ink macrostructure surface: pristine (left), laser-activated (right). SEM micrographs of pristine (**ii**) and laser-treated (**iii**) inks; in-lens signal acquisition magnification 5 kX. Insets report micrographs acquired at Mag 30 kX.

removal of this polymeric coating, unveiling the conductive graphitic matrix, where the overall structure results in more wrinkles and more resolved carbon nanoparticles (iii). The WB-ink pristine morphology provides a possible explanation for the peculiar Raman spectrum obtained, where the low I_D/I_G ratio is probably caused by the superficial resin rather than the graphitic component; Fig. S3 demonstrates how this surface coating removal starts from the lower laser-power applied (1.2 W) in agreement with Raman spectroscopy.

Untreated and laser-treated inks were also investigated via ATR-FTIR (Fig. S4). FTIR spectra returned different signatures for the two inks. In particular, the laser treatment did not result in significant changes for the SB-ink, suggesting that the laser drives a morphological change of the ink rather than of surface chemistry. The treated WB-ink showed an overall increase in all the stretching signals compared with the pristine ink. This result further confirms that the laser induces the removal of the polymeric coating that hides the FT-IR signals of the graphitic material.

To have a broader vision of the laser treatment effect, an accurate electrochemical characterization of the ink-based sensors was carried out, comparing the inks treated with the optimal laser power (4.8 W and 3.6 W for SB and WB ink, respectively) with the pristine inks. To this aim, additional experiments with $[Fe(CN)_6]^{3-/4-}$ were performed to evaluate the main electrochemical parameters (i.e., ECSA and K^0), the double-layer capacitance (C_S), and the electrochemical behavior of model electroactive molecules (i.e., ascorbic acid, caffeic acid and dopamine). The main findings of these studies are discussed below, while the obtained data are reported in full in *section SM.3.1.3*.

Fig. S5 shows the treated and untreated ink comparison and the scan rate study performed with $[Fe(CN)_6]^{3-/4-}$ used to extrapolate the electroactive surface area (ECSA) and the heterogeneous electron transfer rate (k^0) (Bard and Faulkner, 2002; Blandón-Naranjo et al., 2018; Flavio et al., 2020; Nicholson, 1965). Laser-treated inks returned improved ECSAs: SB-ink and WB-ink returned ECSA ~2-fold and ~4-fold higher compared to the untreated inks, respectively. Also k^0 resulted improved after laser treatments for both inks probably due to the larger exposed surface area or surface activation induced. Interestingly, WB-ink underwent a tremendous boost of performance after laser treatment, probably due to the removal of the passivating polymeric coating which hinders the electron transfer with the redox probe.

Fig. S6 reports CVs at increasing scan rates in 1 M KOH, employed to extrapolate the C_S (Voiry et al., 2018). A different behavior was recorded for the two inks in this case. C_S was reduced for SB-ink, while it was markedly (5-fold) increased for WB-ink. The effect observed for the SB-ink has been already described and is attributed to the removal of binders/stabilizers present in the solvent-based ink formulation (Rocha et al., 2021; Yuan et al., 2021). These contribute to the capacitance of the pristine ink, thus their removal induces a C_S decrease. In the case of WB-ink, the C_S increase may be attributed again to the removal of the pristine polymeric matrix, which does not allow efficient charge storage at the electrode/electrolyte interface.

In order to have a better idea about the electrochemical potentiality of the laser-treated inks, electro-active compounds with well-known behavior, namely ascorbic acid, caffeic acid, and dopamine were tested (Fig. S7). Interestingly, the laser treatment for the SB-ink resulted in an overall slight improvement of the performance, particularly for ascorbic acid. On the other hand, the laser-treated WB-ink showed a tremendous improvement in the response, in terms of faradaic current intensity, peak resolution, and signal-to-noise ratio; in this case, the pristine WB-ink was unable to properly react with model compounds. After the laser treatment, the ink displayed a huge boost due to the demasking of the graphitic nanostructure, accompanied by a significant reduction of the faradaic/capacitive current ratio.

Hence, the improvement of the electrochemical performance of the SB-ink can be ascribed to the laser-induced removal of the binders/stabilizers present in the ink native formulation (Alba et al., 2021a; Martin and Claverie, 2022), along with favorable morpho-chemical changes, which results in larger electro-active area and electron-transfer ability. On the other hand, the laser treatment of the WB-ink drives a graphitic nanostructure demasking that results in favorable dramatic changes of physico-chemical and electrochemical features. Moreover, in this case, higher laser power induces additional effects on the conductive graphitic-based component, further improving the charge-transfer properties of the material.

3.2. Catalytic and bioelectroanalytical performance of laser-activated printed inks

The effect of laser activation on the ink-based transducers toward the DET reaction of the FDH redox enzyme was investigated via CV; measurements were performed in the presence and absence of the substrate using bioreaction conditions established in previous studies (Bollella et al., 2018; Silveri et al., 2023a).

Initially, the influence of the enzyme amount was explored on SB-ink and WB-ink treated with laser power of 4.8 W and 3.6 W, respectively, modifying the sensors with different amounts of FDH from 2 to 300 mU. Fig. S8 displays the difference in catalytic current density (Δj, μA cm^{-2}) obtained for both transducers. Notably, 15 mU of FDH resulted in the highest and most reproducible catalytic response, therefore, this FDH amount was selected for following tests. Interestingly, this FDH amount is significantly smaller compared to the conventionally used for biosensors based on commercial and nanomaterial-modified transducers, which results to be approximately close to 240 mU (Bolella et al., 2018; Bollella et al., 2018; Nazaruk et al., 2014).

The impact of the CO_2 laser power applied to activate the inks was also studied vs. the FDH-induced bioelectrocatalytic event; Fig. 3A and 3B shows the cyclic voltammograms obtained for SB-ink and WB-ink, respectively. Measurements were conducted in non-turnover (acetate buffer) and turnover (10 mM fructose in acetate buffer) conditions. The relative current densities (Δj) values obtained are reported in Fig. 3C (SB-ink) and 3D (WB-ink); Δj was extrapolated at +0.25 V (vs Ag/AgCl) to consider the whole electro-catalytic curve (Bollella et al., 2021).

The laser treatment allows pronounced enhancement of the biocatalytic event that results in an exponential increase of the catalytic density current under increasing laser power applied. The maximum of Δj was reached at 4.8 W for the SB-ink (Δj = 120.6 ± 4.3 μA cm^{-2}; E onset = −0.061 V) and 3.6 W for the WB-ink (Δj = 202.0 ± 0.7 μA cm^{-2}; E onset = −0.073 V). Noteworthy, in particular for the WB-ink, the laser acts as an activator since the pristine ink is not able to directly communicate with the FDH; as already discussed in *section 3.1*, the external polymeric coating hinders the interaction with the enzyme redox site. Even the lowest power values used enable the DET reaction. On the other hand, an outstanding catalytic improvement was reached for the SB-ink, where the laser treatment allowed a ~20-fold increase of the Δj compared to the pristine ink (untreated SB-ink Δj = 5.9 ± 0.5 μA cm^{-2}; E_{onset} = +0.015 V). It is interesting to observe that the electrocatalytic waves obtained in turnover conditions for the most performing biosensors are characterized by a shoulder at ~+0.1 V (vs Ag/AgCl), which is attributed to the electron release from the heme group 2c of the subunit II of the enzyme (Bollella et al., 2018, 2021; Silveri et al., 2023a), confirming the ability of the laser-induced effect to drive the FDH DET-based event.

It is also worth noting that the application of higher laser power further boosted the electrocatalysis for both inks, probably due to the additional morpho-chemical changes discussed in *section 3.1*: indeed, the demasking of the graphitic structures together with a laser-driven additional nano-/microstructuration enhance the electron-transfer process ensuring faster electron kinetics. In addition, the removal of binders/coating from the inks probably helps in shortening the distance between the redox site and the transducer surface. Overall, the laser-driven catalysis improvement appears one order of magnitude higher than the crude increase of heterogeneous electron transfer rate (*section 3.1*). Both ink-based FDH sensors, under optimal laser power conditions, gave a reproducible response (SB-ink Δj RSD = 3.6%, WB-ink Δj RSD =

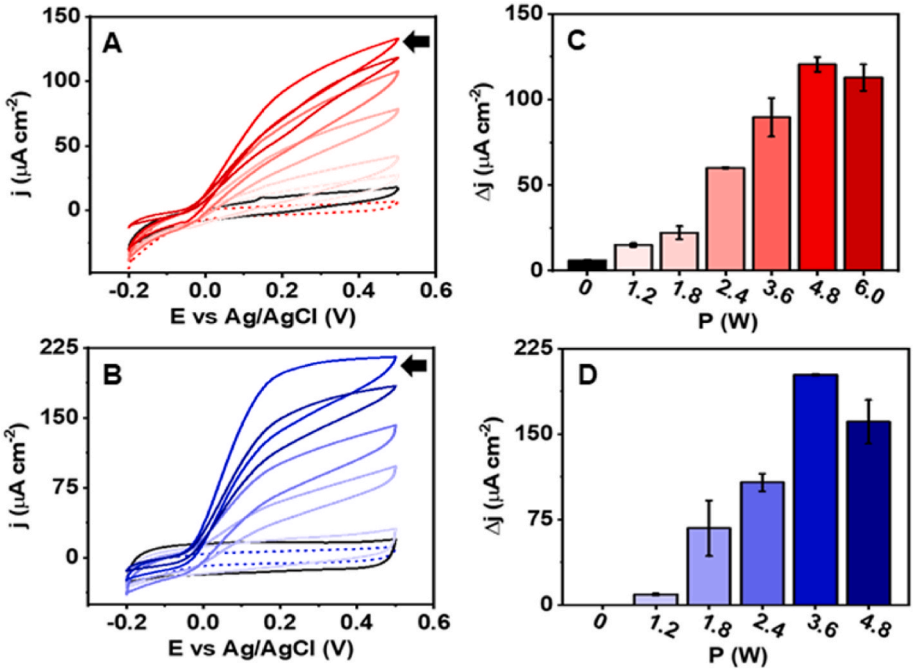

Fig. 3. Cyclic voltammograms and relative current densities (Δj; recorded at +0.25 V vs Ag/AgCl) obtained for SB (**A-C**) and WB (**B-D**) ink transducers treated with different laser beam powers and modified with 15 mU of FDH. Measurements were carried out in the presence (full curves) and absence of 10 mM D-fructose (dashed curves). The curves obtained in absence of D-fructose are reported only for laser power of 4.8 W and 3.6 W for SB and WB ink, respectively. The laser power increase (from 1.2 to 6 W) is indicated by the relative color darkening; black curves and bars represent untreated transducers. Δj values were calculated subtracting the capacitive current of the relative blank (acetate buffer) from the faradaic catalytic current obtained in presence of D-fructose; CV scan rate 5 mV s^{-1}.

0.4%; n = 3), further proving the ability of the laser-treated inks to accommodate the FDH in a favorable and reproducible way.

Kinetics and analytical figures of merit were then investigated via amperometry using all-in-one integrated ink-based biosensors (*section 2.3*) activated with the different laser power (0, 1.2, 1.8, 2.4, 3.6, 4.8, 6.0 W); an overpotential of +0.15 V (vs. pseudo-Ag/AgCl) was employed, working in diffusion control under continuous addition of D-fructose from 1 μM to 60 mM. Fig. 4A and 4**B** report the obtained amperometry plots for SB-ink and WB-ink, respectively, while the extrapolated dose-response curves are shown in Fig. 4C and **D**.

Regardless of the applied laser power, SB-ink and WB-ink biosensors exhibited a Michaelis-Menten behavior, with K_m^{app} values in the 7.3–10.7 mM range, in agreement with the literature (Bolella et al., 2018; Bollella et al., 2018; Silveri et al., 2023a). The extrapolated j_{max} trend is

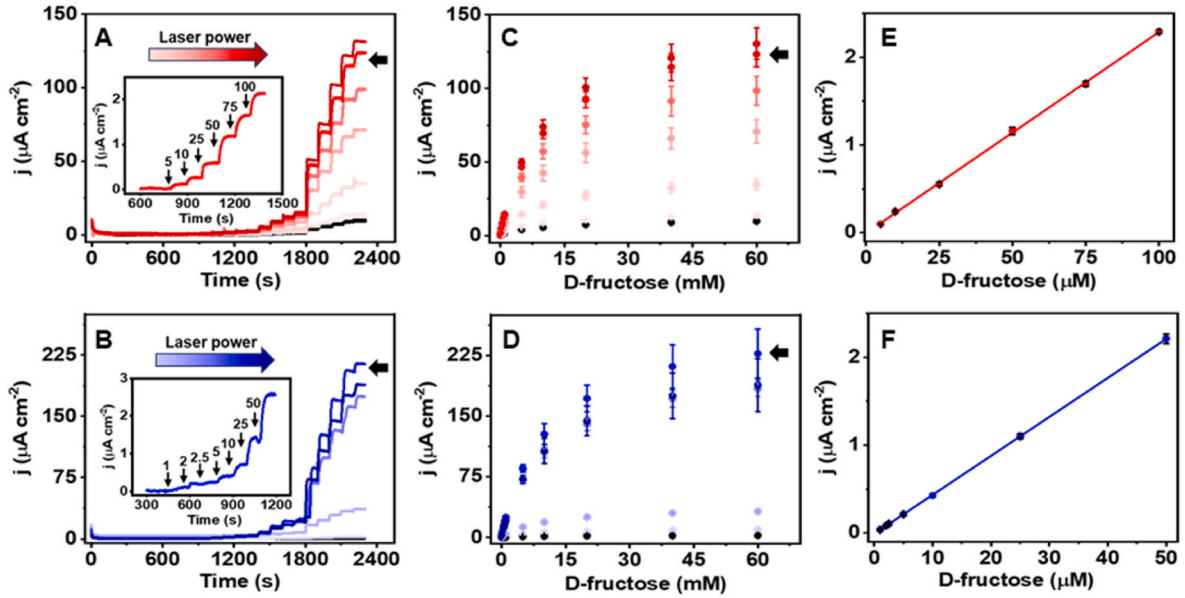

Fig. 4. Amperometric measurements and relative dose-response curves obtained under continuous addition of increasing concentrations of D-fructose (1 μM - 60 mM) for SB (**A**, **C**, **E**) and WB (**B**, **D**, **F**) ink transducers treated with different laser beam powers modified with 15 mU of FDH. The laser power increase (from 1.2 to 6 W) is indicated by the relative color darkening; black curves and points represent untreated transducers. D-fructose concentrations reported in the A and B insets are expressed in μM and are referred to laser-activated biosensors obtained at 4.8 W (LSB-FDH) and 3.6 W (LWB-FDH). Linear plots for LSB-FDH (**E**; L.P. 4.8 W) and LWB-FDH (**F**; L.P. 3.6 W); operating potential +0.15 V vs. pseudo-Ag/AgCl.

consistent with the previously observed electro-catalytic curves, indeed the j_{max} increase in function of the laser power applied, showing the maximum at 4.8 W for the SB-ink ($j_{max} = 143.9 \pm 1.7$ μA cm^{-2}) and at 3.6 W for WB-ink ($j_{max} = 266.7 \pm 2.0$ μA cm^{-2}); applying highers laser powers lower values were observed. Also in this case, the pristine WB-ink failed to work, while an outstanding catalytic improvement was reached for the SB-ink, where the laser treatment allowed to improve ~15-fold J_{max} with respect to the pristine-ink (untreated SB-ink $J_{max} = 10.8 \pm 0.3$ μA cm^{-2}).

Analytical features were studied focusing on the linear range of response extrapolated from the dose-response curves of the most performing laser-activated biosensors, from now named LSB-FDH and LWB-FDH. Fig. 4E and 4**F** report the linear plots for laser-activated LSB-FDH (5–100 μM) and LWB-FDH (1–50 μM) obtained for D-fructose, respectively. The limits of detection (LODs) and sensitivity achieved were 0.47 μM and 22.90 ± 0.62 μA cm^{-2} mM^{-1} for LSB-FDH, and 0.24 μM and 44.40 ± 0.82 μA cm^{-2} mM^{-1} for LWB-FDH. LOD was calculated using the formula 3σ/m (σ = standard deviation of the intercept; m = mean value of the slope). Reproducibility of the biosensors was calculated from calibration curves obtained with three independent electrodes: both biosensors showed an extremely satisfactory inter-electrode precision (LSB-FDH slope: 0.0229 ± 0.0006 μA cm^{-2} μM^{-1}, RSD = 2.7%; LWB-FDH slope: 0.0444 ± 0.0008 μA cm^{-2} μM^{-1}, RSD = 1.8%; n = 3), endorsing the robustness of the laser-activation and biosensors manufacturing procedure.

Taking a look at the literature, pioneering works reported the use of laser treatments to improve the electrochemical features of graphitic inks toward the electroanalysis of different electro-active compounds and redox probes (Alba et al., 2021a, 2021b). Other works used laser to construct supercapacitors (Baptista et al., 2022) and electrochemiluminescence devices (Alba et al., 2022), whereas there are no examples of laser-treated inks for the development of DET-type 3rd-generation enzymatic sensors.

Overall, the laser approach emerged among printed electrode activation strategies. In particular, compared to the more conventional anodization (Paimard et al., 2023; Rana et al., 2019), which is based on the changing of the sensing surface chemistry, the laser activation drives printed ink structural/chemical changes (as discussed in *section 3.1*), particularly effective in favoring DET catalysis. In this regard, to the best of our knowledge, there are no studies where anodization treatments of conductive inks were exploited to activate/improve FDH-based sensors.

Table S1 summarizes FDH-based sensors present in the literature; they rely mainly on the use of conventional transducers (glassy carbon, porous gold, carbon paste, etc.) which require chemical functionalization to guide the orientation of the redox protein, while the use of printed transducers is poorly explored. The latter strategy is reported in a previous work of our group where to reach the desired features, the lab-made electrodes were modified with different kinds of nanomaterials (Silveri et al., 2023a). The latter needs to be properly synthesized, purified, and carefully used to modify the sensing surface.

The proposed laser-based approach allowed to obtain competitive analytical performance compared with the literature, resulting smart, capable of in-series production of 3rd generation enzymatic biosensors, and prone to be further automatized and scaled up. For the sake of clarity, it must be pointed out that, despite the advantages, laser-based strategies may present some limitations; in fact, the laser treatments do not work for any surface and need to be carefully optimized according to the substrate and the analytical performances required.

3.3. D-fructose determination and in-continuous monitoring in biological fluids

D-fructose levels in biological fluids are markers for various physiological functions (Andres-Hernando et al., 2019). D-fructose in high quantities in seminal fluid is associated to a good state of health, although its correlation with fertility and sperm mobility is not fully understood (Johnson et al., 2020; Shemshaki et al., 2021). Endogenous increase of D-fructose levels in cerebrospinal fluid has been linked to different toxic effects, particularly in diabetic individuals (Tigchelaar et al., 2022). On the other hand, high D-fructose intake from the diet has been associated to adverse health effects for infants affected by hereditary fructose intolerance (Li et al., 2018; Singh and Sarma, 2022); despite this, D-fructose is employed in some infant milk formulations, even though discouraged by the World Health Organization (WHO) (Awad et al., 2022; Koletzko et al., 2005; Scano et al., 2016).

In this framework, laser-activated ink-based FDH biosensors were challenged for D-fructose determination in synthetic biological fluids and surrogate breast milk. Firstly, the selectivity of the biosensors was studied, evaluating potential interfering species present in these matrices. Fig. 5A reports the amperometric response to D-fructose, before and after the addition of organic compounds (**5Ai**), salts (**5Aii**), mono/disaccharides (**5Aiii**), and vitamins (**5Aiv**). These compounds were selected according to the literature (Awad et al., 2022; Scano et al., 2016), taking into account the sample dilution needed for the D-fructose analysis; the complete list and the concentration of the tested species are reported in the figure caption.

The biosensors' response was not affected by potentially electroactive organic compounds and vitamins, thanks to the features of the ink-based biosensors that allowed working at low overpotential. No signal perturbation was recorded in the presence of salts, whereas high selectivity toward sugars is ascribable to the FDH specificity for D-fructose. Noteworthy, D-fructose returns the same current intensity in absence and presence of the interfering species (relative signal recovery ≤93.5%), further endorsing the selectivity and proving the ability of the biosensor to work in complex matrices.

Also artificial seminal fluid (aSF) and synthetic cerebrospinal fluid (CSF) used to simulate biological fluids, were analyzed via amperometry (*section 2.6*) using LSB-FDH and LWB-FDH biosensors; the samples were fortified upstream, and three levels were employed to mimic the endogenous fructose content of D-fructose (i.e. 5, 10, and 15 mM for aSF and 100, 300, and 500 μM for SCF). Powder formula milk and lyophilized donkey milk were tested as breastfeeding surrogates, in this case, the raw' samples were fortified at 250, 375, and 500 μM according to the literature (Awad et al., 2022; Scano et al., 2016). Fig. 5B and 5C depict examples of amperometry plots obtained with synthetic biological fluids and powder milk, respectively, whereas Table S2 lists the complete data set obtained; the standard additions method was used for the D-fructose quantification. Satisfactory recoveries were achieved for all the samples using both biosensors (LSB-FDH 93–107%, LWB-FDH 96–112%), accompanied by an acceptable reproducibility (LSB-FDH RSD ≤8.0%, LWB-FDH RSD ≤7.9%; n = 3), endorsing the laser-activated biosensors exploitability in real-world D-fructose analysis.

Eventually, the ink-based biosensors were challenged for the continuous monitoring of D-fructose in CSF. The D-fructose-induced fluctuations, detailed described in *section SM.2.6*, were settled to replicate the fluctuations occurring in the brain associated with the polyol pathway (Hwang et al., 2017). The latter is activated by the accumulation of D-glucose, which is subsequently converted into D-fructose (Andres-Hernando et al., 2019; Garg and Gupta, 2022). This metabolic pathway is associated with negative health effects particularly relevant for diabetic patients (Hwang et al., 2017; Tigchelaar et al., 2022).

Fig. 5D displays the amperometry plots obtained for the in-continuous D-fructose measurements in CSF using the LSB-FDH (red-line) and LWB-FDH (blue-line) biosensors. Two potential physiological conditions were simulated, i.e., (i) initial condition with no D-fructose in the brain, (ii) initial condition with high levels of D-Fructose present in the CSF. In both cases, along the 1.5 h of measure, two additional D-fructose fluctuations have been induced (see *section SM.2.6*). Laser-treated ink-based biosensors result able to continuously track D-fructose, returning currents consistent with the sugar concentration, resulting also able to point out fluctuations occurring after 1 h of continuous measure; moreover, satisfactory stability of the

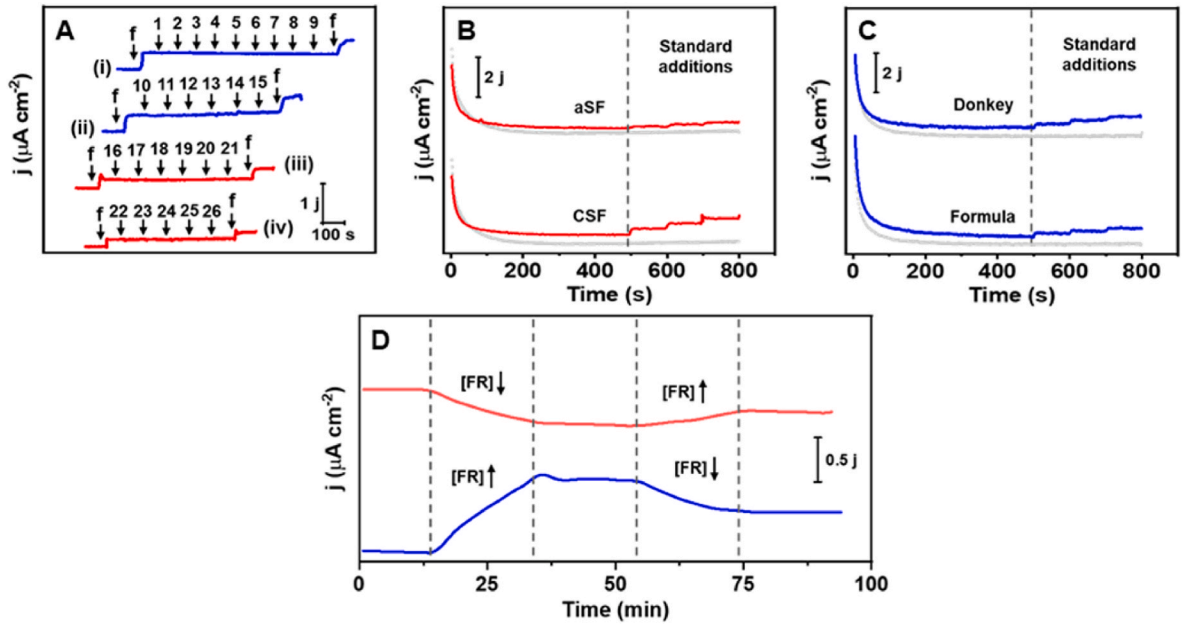

Fig. 5. Selectivity study and D-fructose determination in samples. (**A**) Amperometry plots obtained with LSB-FDH (red curves) and LWB-FDH (blue curves) biosensors under continuous addition of potential interfering species, 'f' stands for 10 μM D-fructose. (**i**) 1 (1 mM urea), 2 (1 mM citric acid), 3 (50 μM L-carnitine), 4 (50 μM choline), 5 (50 μM uric acid), 6 (25 μM glutamic acid), 7 (50 μM lactic acid), 8 (100 μM bovine serum albumin), 9 (1 μM dopamine). (**ii**) 10 (1 mM $CaCl_2$), 11 (1 mM $MgCl_2$), 12 (1 mM $ZnCl_2$), 13 (1 mM NaCl), 14 (1 mM K_2HPO_4), 15 (1 mM $CaCO_3$). (**iii**) 16 (1 mM lactose), 17 (1 mM D-glucose), 18 (1 mM sorbitol), 19 (1 mM sucrose), 20 (1 mM D-galactose), 21 (1 mM D-fucose). (**iv**) 22 (25 μM niacin), 23 (25 μM pyridoxal), 24 (25 μM biotin), 25 (25 μM nicotinic acid), 26 (5 μM ascorbic acid). (**B**) LSB-FDH biosensor amperometry plots for aSF and CSF fortified upstream with 10 mM and 300 μM D-fructose, respectively; (**C**) LWB-FDH biosensor amperometry plots for donkey powder milk and formula milk fortified in matrix with 375 μM D-fructose. Standard additions in samples were performed by adding three times consecutively 10 μM of D-fructose (5 μM for CSF); grey curves represent blank measures. Samples dilution in acetate buffer (v/v): aSF 1:1000, CSF 1:10, formula and donkey powder milk 1:50. (**D**) Amperometry plots for in-continuous D-fructose measurements in CSF using the LSB-FDH (red-line) and LWB-FDH (blue-line) biosensors; the detailed flows and D-fructose induced fluctuation are reported in section SM.2.6. All amperometries were conducted at +0.15 V vs pseudo-Ag/AgCl.

amperometry response was observed during the 'stationary' phases (D-fructose level kept constant).

This is the first time that the ability of FDH-based sensors to perform continuous measurement of D-fructose in a complex medium has been proved, opening new options for real-time analysis in biological fluids. Overall, the sample analysis output is very relevant considering that, to the best of our knowledge, none of the existing FDH-based electrochemical sensors (summarized in Table S1) has been employed to analyze these biological matrices.

4. Conclusions

A CO_2-laser approach to activate/boost printed-electronic direct enzymatic bioelectrocatalysis is successfully proposed and exploited to build lab-made biosensors for D-fructose analysis in biological fluids. Laser treatment, studied on different printed inks, proved to activate/improve direct electron transfer biocatalysis, thanks to a combination of morpho-chemical variations, and is function of the applied laser power. Optimized laser treatments ensure faster electron kinetics, bringing out underlying graphitic structures that are also additionally nano-/micro-structured; these effects maximize the ability to host the FDH, improving the capacity to draw electrons from the enzyme active site. The complete laser-activated fructose dehydrogenase-based biosensors revealed competitive performance comparably to more complex nanomaterial-based biosensors, working at low-overpotential, sub-μmolar limits of detection were obtained. The biosensors' features allowed to determine D-fructose in synthetic and real biological fluids, proving also the ability to work for continuous monitoring in simulated physiological D-fructose fluctuations in cerebrospinal fluid.

Summing up, the proposed laser-based strategy allows to activate/boost lab-produced printed electronics in a few seconds, unveiling useful electroanalytical and biocatalytic features, becoming a fast and scalable tool to manufacture in-serie performing sensors and biosensors.

CRediT authorship contribution statement

Filippo Silveri: Writing – original draft, Visualization, Methodology, Investigation, Formal analysis, Data curation, Conceptualization. **Flavio Della Pelle:** Writing – review & editing, Validation, Supervision, Project administration, Investigation, Data curation, Conceptualization. **Annalisa Scroccarello:** Writing – review & editing, Visualization, Software, Methodology, Conceptualization. **Paolo Bollella:** Writing – review & editing, Validation, Methodology, Formal analysis. **Giovanni Ferraro:** Writing – review & editing, Visualization, Methodology, Investigation. **Eole Fukawa:** Resources, Methodology, Investigation. **Yohei Suzuki:** Resources, Methodology, Investigation. **Keisei Sowa:** Writing – review & editing, Validation, Resources, Methodology, Investigation. **Luisa Torsi:** Writing – review & editing. **Dario Compagnone:** Writing – review & editing, Supervision, Resources, Funding acquisition, Formal analysis.

Declaration of competing interest

The authors declare that they have no known competing financial interests or personal relationships that could have appeared to influence the work reported in this paper.

Data availability

Data will be made available on request.

Acknowledgments

The authors acknowledge financial support of MUR PRIN 2022 Project No. 2022T2E7NT_01, CUP C53D23003850006, under the National Recovery and Resilience Plan (NRRP), Mission 4 Component C2 Investment 1.1-MUR call No. 104 on February 2, 2022, funded by the European Union-NextGenerationEU. G.F. acknowledge Consorzio per lo sviluppo dei Sistemi a Grande Interfase (CSGI) for financial support. This research was supported by JSPS KAKENHI, Grant Number JP22K14831 to KS.

Appendix A. Supplementary data

Supplementary data to this article can be found online at https://doi.org/10.1016/j.bios.2024.116620.

References

Adachi, T., Kitazumi, Y., Shirai, O., Kano, K., 2020. Direct electron transfer-type bioelectrocatalysis of redox enzymes at nanostructured electrodes. Catalysts 10. https://doi.org/10.3390/catal10020236.

Alba, A.F., Totoricaguena-Gorrino, J., Campos-Arias, L., Peřinka, N., Ruiz-Rubio, L., Vilas-Vilela, J.L., Lanceros-Méndez, S., Del Campo, F.J., 2021a. Laser-induced highly oriented pyrolytic graphite for high-performance screen-printed electrodes. Mater. Adv. 2, 5912–5921. https://doi.org/10.1039/d1ma00582k.

Alba, A.F., Totoricaguena-Gorriño, J., Sánchez-Ilárduya, M.B., Ruiz-Rubio, L., Vilas-Vilela, J.L., Lanceros-Méndez, S., del Campo, F.J., 2021b. Laser-activated screen-printed carbon electrodes for enhanced dopamine determination in the presence of ascorbic and uric acid. Electrochim. Acta 399, 139374. https://doi.org/10.1016/j.electacta.2021.139374.

Alba, A.F., Fernández-de Luis, R., Totoricaguena-Gorriño, J., Ruiz-Rubio, L., Sánchez, J., Vilas-Vilela, J.L., Lanceros-Méndez, S., del Campo, F.J., 2022. Understanding electrogenerated chemiluminescence at graphite screen-printed electrodes. J. Electroanal. Chem. 914, 116331 https://doi.org/10.1016/j.jelechem.2022.116331.

Andres-Hernando, A., Johnson, R.J., Lanaspa, M.A., 2019. Endogenous fructose production: what do we know and how relevant is it? Curr. Opin. Clin. Nutr. Metab. Care 22, 289–294. https://doi.org/10.1097/MCO.0000000000000573.

Awad, R., Kowash, M., Hussein, I., Salami, A., Abdo, M., Al-Halabi, M., 2022. Sugar content in infant formula : accuracy of labeling and conformity to guidelines. Int. J. Paediatr. Dent. 63–73. https://doi.org/10.1111/ipd.13014.

Baptista, M., Gaspar, G., Wijayantha, K.G.U., Lobato, K., 2022. The impact of laser-scribing carbon-based supercapacitor electrodes. Appl. Surf. Sci. Adv. 10, 100262 https://doi.org/10.1016/j.apsadv.2022.100262.

Bard, A.J., Faulkner, L.R., 2002. Electrochemical methods: fundamentals and applications. Russ. J. Electrochem. 38, 1364–1365. https://doi.org/10.1023/A:1021637209564.

Blandón-Naranjo, L., Della Pelle, F., Vázquez, M.V., Gallego, J., Santamaría, A., Alzate-Tobón, M., Compagnone, D., 2018. Electrochemical behaviour of microwave-assisted oxidized MWCNTs based disposable electrodes: proposal of a NADH electrochemical sensor. Electroanalysis 30, 509–516. https://doi.org/10.1002/elan.201700674.

Bolella, P., Hibino, Y., Kano, K., Gorton, L., Antiochia, R., 2018. Enhanced DET of FDH rationally immobilized on a 2-aminoanthracene diazonium cation. ACS Catal. 8, 10279–10289.

Bollella, P., 2022. Enzyme-based amperometric biosensors: 60 years later … Quo Vadis? Anal. Chim. Acta 1234, 340517. https://doi.org/10.1016/j.aca.2022.340517.

Bollella, P., Katz, E., 2020. Enzyme-based biosensors: tackling electron transfer issues. Sensors 20, 1–32. https://doi.org/10.3390/s20123517.

Bollella, P., Hibino, Y., Kano, K., Gorton, L., Antiochia, R., 2018. Highly sensitive membraneless fructose biosensor based on fructose dehydrogenase immobilized onto aryl thiol modified highly porous gold electrode: characterization and application in food samples. Anal. Chem. 90, 12131–12136. https://doi.org/10.1021/acs.analchem.8b03093.

Bollella, P., Boeva, Z., Latonen, R.M., Kano, K., Gorton, L., Bobacka, J., 2021. Highly sensitive and stable fructose self-powered biosensor based on a self-charging biosupercapacitor. Biosens. Bioelectron. 176, 112909 https://doi.org/10.1016/j.bios.2020.112909.

Camargo, J.R., Orzari, L.O., Araújo, D.A.G., de Oliveira, P.R., Kalinke, C., Rocha, D.P., Luiz dos Santos, A., Takeuchi, R.M., Munoz, R.A.A., Bonacin, J.A., Janegitz, B.C., 2021. Development of conductive inks for electrochemical sensors and biosensors. Microchem. J. 164 https://doi.org/10.1016/j.microc.2021.105998.

Cheunkar, S., Oaew, S., Parnsubsakul, A., Asanithi, P., 2022. Reactive argon-plasma activation of screen-printed carbon electrodes for highly selective dopamine determination. Anal. Methods 14, 4193–4201. https://doi.org/10.1039/d2ay01154a.

Dave, Pranav Y., 2020. Short review on printing ink technology to prevent counterfeit of the products. J. Adv. Chem. Sci. 6, 693–697. https://doi.org/10.30799/jacs.227.20060401.

Della Pelle, F., Bukhari, Q.U.A., Álvarez-Diduk, R., Scroccarello, A., Compagnone, D., Merkoçi, A., 2023. Freestanding laser-induced two dimensional heterostructures for self-contained paper-based sensors. Nanoscale 15, 7164–7175. https://doi.org/10.1039/d2nr07157f.

Dimitriou, E., Michailidis, N., 2021. Printable conductive inks used for the fabrication of electronics: an overview. Nanotechnology 32. https://doi.org/10.1088/1361-6528/abefff.

Ferrari, A.C., 2007. Raman spectroscopy of graphene and graphite: disorder, electron-phonon coupling, doping and nonadiabatic effects. Solid State Commun. 143, 47–57. https://doi.org/10.1016/j.ssc.2007.03.052.

Flavio, D.P., Daniel, R., Filippo, S., Giovanni, F., Emiliano, F., Annalisa, S., Alberto, E., Dario, C., 2020. Class-selective voltammetric determination of hydroxycinnamic acids structural analogs by using a WS2/catechin-capped-AuNPs/carbon black based nanocomposite sensor. Microchim. Acta. 187, 1–13. https://doi.org/10.1007/s00604-020-04281-z.

Fukawa, E., Suzuki, Y., Adachi, T., Miyata, T., Makino, F., Tanaka, H., Namba, K., Sowa, K., Kitazumi, Y., Shirai, O., 2024. Structural and electrochemical elucidation of biocatalytic mechanisms in direct electron transfer-type D-fructose dehydrogenase. Electrochim. Acta 490, 144271. https://doi.org/10.1016/j.electacta.2024.144271.

Garg, S.S., Gupta, J., 2022. Polyol pathway and redox balance in diabetes. Pharmacol. Res. 182, 106326 https://doi.org/10.1016/j.phrs.2022.106326.

Griffiths, K., Dale, C., Hedley, J., Kowal, M.D., Kaner, R.B., Keegan, N., 2014. Laser-scribed graphene presents an opportunity to print a new generation of disposable electrochemical sensors. Nanoscale 6, 13613–13622. https://doi.org/10.1039/c4nr04221b.

Hwang, J.J., Jiang, L., Hamza, M., Dai, F., Belfort-DeAguiar, R., Cline, G., Rothman, D.L., Mason, G., Sherwin, R.S., 2017. The human brain produces fructose from glucose. JCI Insight 2, 1–6. https://doi.org/10.1172/jci.insight.90508.

Johnson, J., Flores, M.G., Rosa, J., Han, C., Salvi, A.M., DeMali, K.A., Jagnow, J.R., Sparks, A., Haim, H., 2020. The high content of fructose in human semen competitively inhibits broad and potent antivirals that target high-mannose glycans. J. Virol. 94 https://doi.org/10.1128/jvi.01749-19.

Kawai, S., Goda-Tsutsumi, M., Yakushi, T., Kano, K., Matsushita, K., 2013. Heterologous overexpression and characterization of a flavoprotein-cytochrome c complex fructose dehydrogenase of Gluconobacter japonicus NBRC3260. Appl. Environ. Microbiol. 79, 1654–1660. https://doi.org/10.1128/AEM.03152-12.

Kay, R., Desmulliez, M., 2012. A review of stencil printing for microelectronic packaging. Solder. Surf. Mt. Technol. 24, 38–50. https://doi.org/10.1108/09540911211198540.

Koletzko, B., Baker, S., Cleghorn, G., Neto, U.F., Gopalan, S., Hernell, O., Hock, Q.S., Jirapinyo, P., Lonnerdal, B., Pencharz, P., Pzyrembel, H., Ramirez-Mayans, J., Shamir, R., Turck, D., Yamashiro, Y., Zong-Yi, D., 2005. Global standard for the composition of infant formula: recommendations of an ESPGHAN coordinated international expert group. J. Pediatr. Gastroenterol. Nutr. 41, 584–589.

Kongkaew, S., Tubtimtong, S., Thavarungkul, P., Kanatharana, P., Chang, K.H., Abdullah, A.F.L., Limbut, W., 2022. A fabrication of multichannel graphite electrode using low-cost stencil-printing technique. Sensors 22, 1–13. https://doi.org/10.3390/s22083034.

Li, H., Byers, H.M., Diaz-Kuan, A., Vos, M.B., Hall, P.L., Tortorelli, S., Singh, R., Wallenstein, M.B., Allain, M., Dimmock, D.P., Farrell, R.M., McCandless, S., Gambello, M.J., 2018. Acute liver failure in neonates with undiagnosed hereditary fructose intolerance due to exposure from widely available infant formulas. Mol. Genet. Metabol. 123, 428–432. https://doi.org/10.1016/j.ymgme.2018.02.016.

Ma, B., Rodrigues, R.D., Ruban, A., Pavlov, S., Sheremet, E., 2019. The correlation between electrical conductivity and second-order Raman modes of laser-reduced graphene oxide. Phys. Chem. Chem. Phys. 21, 10125–10134. https://doi.org/10.1039/C9CP00093C.

Marchianò, V., Tricase, A., Caputo, M., Farinini, E., Leardi, R., Imbriano, A., Leech, D., Kidayaveettil, R., Gentile, L., Torsi, L., Macchia, E., Bollella, P., 2024. Tailoring water-based graphite conductive ink formulation for enzyme stencil-printing: experimental design to enhance wearable biosensor performance. Chem. Mater. 36, 358–370. https://doi.org/10.1021/acs.chemmater.3c02229.

Martin, B., Claverie, J.P., 2022. Depolymerizable polyimines triggered by heat or acid as binders for conductive inks. ACS Appl. Polym. Mater. 4, 4912–4918. https://doi.org/10.1021/acsapm.2c00491.

Martins, P., Pereira, N., Lima, A.C., Garcia, A., Mendes-Filipe, C., Policia, R., Correia, V., Lanceros-Mendez, S., 2023. Advances in printing and electronics: from engagement to commitment. Adv. Funct. Mater. 33 https://doi.org/10.1002/adfm.202213744.

Nazaruk, E., Landau, E.M., Bilewicz, R., 2014. Membrane bound enzyme hosted in liquid crystalline cubic phase for sensing and fuel cells. Electrochim. Acta 140, 108–115. https://doi.org/10.1016/j.electacta.2014.05.130.

Nicholson, R.S., 1965. Theory and application of cyclic voltammetry for measurement of electrode reaction kinetics. Anal. Chem. 37, 1351–1355.

Paimard, G., Ghasali, E., Baeza, M., 2023. Screen-printed electrodes: fabrication, modification, and biosensing applications. Chemosensors 11. https://doi.org/10.3390/chemosensors11020113.

Rana, A., Baig, N., Saleh, T.A., 2019. Electrochemically pretreated carbon electrodes and their electroanalytical applications – a review. J. Electroanal. Chem. 833, 313–332. https://doi.org/10.1016/j.jelechem.2018.12.019.

Rocha, D.P., Ataide, V.N., de Siervo, A., Gonçalves, J.M., Muñoz, R.A.A., Paixão, T.R.L.C., Angnes, L., 2021. Reagentless and sub-minute laser-scribing treatment to produce enhanced disposable electrochemical sensors via additive manufacture. Chem. Eng. J. 130594 https://doi.org/10.1016/j.cej.2021.130594.

Sanchez-Duenas, L., Gomez, E., Larrañaga, M., Blanco, M., Goitandia, A.M., Aranzabe, E., Vilas-Vilela, J.L., 2023. A review on sustainable inks for printed electronics: materials for conductive, dielectric and piezoelectric sustainable inks. Materials 16. https://doi.org/10.3390/ma16113940.

Scano, P., Murgia, A., Demuru, M., Consonni, R., Caboni, P., 2016. Metabolite profiles of formula milk compared to breast milk. Food Res. Int. 87, 76–82. https://doi.org/10.1016/j.foodres.2016.06.024.

Schachinger, F., Chang, H., Scheiblbrandner, S., Ludwig, R., 2021. Amperometric biosensors based on direct electron transfer enzymes. Molecules 26. https://doi.org/10.3390/molecules26154525.

Scroccarello, A., Ruslan, A., Pelle, F. Della, Carvalho, C. De, Idili, A., Parolo, C., Compagnone, D., Merkoc, A., 2023. One-step laser nanostructuration of reduced graphene oxide films embedding metal nanoparticles for sensing applications. ACS Sens. 8, 598–609. https://doi.org/10.1021/acssensors.2c01782.

Shemshaki, G., Murthy, A., Malini, S., 2021. Assessment and establishment of correlation between reactive oxidation species, citric acid, and fructose level in infertile male individuals: a machine-learning approach. J. Hum. Reprod. Sci. 14, 129–136. https://doi.org/10.4103/jhrs.jhrs_26_21.

Silva, R. de O., da Silva, É.A., Fiorucci, A.R., Ferreira, V.S., 2019. Electrochemically activated multi-walled carbon nanotubes modified screen-printed electrode for voltammetric determination of sulfentrazone. J. Electroanal. Chem. 835, 220–226. https://doi.org/10.1016/j.jelechem.2019.01.018.

Silveri, F., Paolini, D., Della Pelle, F., Bollella, P., Scroccarello, A., Suzuki, Y., Fukawa, E., Sowa, K., Di Franco, C., Torsi, L., Compagnone, D., 2023a. Lab-made flexible third-generation fructose biosensors based on 0D-nanostructured transducers. Biosens. Bioelectron. 237, 115450 https://doi.org/10.1016/j.bios.2023.115450.

Silveri, F., Scroccarello, A., Pelle, F. Della, Carlo, M. Del, Compagnone, D., 2023b. Rapid pretreatment-free evaluation of antioxidant capacity in extra virgin olive oil using a laser-nanodecorated electrochemical lab-on-strip. Food Chem. 420, 136112–136122. https://doi.org/10.1016/j.foodchem.2023.136112.

Singh, S.K., Sarma, M. Sen, 2022. Hereditary fructose intolerance: a comprehensive review. World J. Clin. Pediatr. 11, 321–329. https://doi.org/10.5409/wjcp.v11.i4.321.

Suresh, R.R., Lakshmanakumar, M., Arockia Jayalatha, J.B.B., Rajan, K.S., Sethuraman, S., Krishnan, U.M., Rayappan, J.B.B., 2021. Fabrication of screen-printed electrodes: opportunities and challenges. J. Mater. Sci. 56, 8951–9006. https://doi.org/10.1007/s10853-020-05499-1.

Suzuki, Y., Makino, F., Miyata, T., Tanaka, H., Namba, K., Kano, K., Sowa, K., Kitazumi, Y., Shirai, O., 2023. Essential insight of direct electron transfer-type bioelectrocatalysis by membrane-bound d-fructose dehydrogenase with structural bioelectrochemistry. ACS Catal. 13, 13828–13837. https://doi.org/10.1021/acscatal.3c03769.

Tigchelaar, C., van Zuylen, M.L., Hulst, A.H., Preckel, B., van Beek, A.P., Kema, I.P., Hermanides, J., Absalom, A.R., 2022. Elevated cerebrospinal fluid glucose levels and diabetes mellitus are associated with activation of the neurotoxic polyol pathway. Diabetologia 65, 1098–1107. https://doi.org/10.1007/s00125-022-05693-7.

Tricase, A., Imbriano, A., Valentino, M., Ditaranto, N., Macchia, E., Di Franco, C., Kidayaveettil, R., Leech, D., Piscitelli, M., Scamarcio, G., Perchiazzi, G., Torsi, L., Bollella, P., 2023. Water-based conductive ink formulations for enzyme-based wearable biosensors. Adv. Sci. News, 2300036.

Veloso, W.B., Ataide, V.N., Rocha, D.P., Nogueira, H.P., de Siervo, A., Angnes, L., Muñoz, R.A.A., Paixão, T.R.L.C., 2023. 3D-printed sensor decorated with nanomaterials by CO2 laser ablation and electrochemical treatment for non-enzymatic tyrosine detection. Microchim. Acta 190, 1–11. https://doi.org/10.1007/s00604-023-05648-8.

Voiry, D., Chhowalla, M., Gogotsi, Y., Kotov, N.A., Li, Y., Penner, R.M., Schaak, R.E., Weiss, P.S., 2018. Best practices for reporting electrocatalytic performance of nanomaterials. ACS Nano 12, 9635–9638. https://doi.org/10.1021/acsnano.8b07700.

You, R., Liu, Y.Q., Hao, Y.L., Han, D.D., Zhang, Y.L., You, Z., 2020. Laser fabrication of graphene-based flexible electronics. Adv. Mater. 32, 1–22. https://doi.org/10.1002/adma.201901981.

Yuan, X., Ma, L., Zhang, J., Zheng, Y., 2021. Simple pre-treatment by low-level oxygen plasma activates screen-printed carbon electrode: potential for mass production. Appl. Surf. Sci. 544, 148760 https://doi.org/10.1016/j.apsusc.2020.148760.

Zappi, D., Varani, G., Cozzoni, E., Iatsunskyi, I., Laschi, S., Giardi, M.T., 2021. Innovative eco-friendly conductive ink based on carbonized lignin for the production of flexible and stretchable bio-sensors. Nanomaterials 11. https://doi.org/10.3390/nano11123428.